Available online at www.sciencedirect.com

jmr&t Journal of Materials Research and Technology

journal homepage: www.elsevier.com/locate/jmrt

Original Article

Influence of heavy metal oxides to the mechanical and radiation shielding properties of borate and silica glass system

M.H.M. Zaid [a,*], H.A.A. Sidek [a], K.A. Matori [a], A. Abdu [b], K.A. Mahmoud [c], Maha M. Al-Shammari [d], E. Lacomme [e], Mohammad A. Imheidat [f], M.I. Sayyed [f,g]

[a] Department of Physics, Faculty of Science, Universiti Putra Malaysia, 43400 UPM, Serdang, Selangor, Malaysia
[b] Department of Forestry Science & Biodiversity, Faculty of Forestry, Universiti Putra Malaysia, 43400, UPM Serdang, Selangor, Malaysia
[c] Ural Federal University, Yekaterinburg, Russia
[d] Computational Unit, Department of Environmental Health, Imam Abdulrahman bin Faisal University, PO Box 1982, Dammam, 31441, Saudi Arabia
[e] Advance Science Research, Junior, Eastchester High School, Eastchester, NY, United States
[f] Department of Physics, Faculty of Science, Isra University, Amman, Jordan
[g] Department of Nuclear Medicine Research, Institute for Research and Medical Consultations (IRMC), Imam Abdulrahman Bin Faisal University (IAU), P.O. Box 1982, Dammam, 31441, Saudi Arabia

ARTICLE INFO

Article history:
Received 23 October 2020
Accepted 27 January 2021
Available online 2 February 2021

Keywords:
Radiation shielding
Glasses
Makishima-Mackenzie model
Elastic properties

ABSTRACT

Six borate and silica glasses with varying compositions were investigated for their mechanical and radiation shielding viability. Makishima-Mackenzie elastic model was utilized to study the elastic properties of the investigated glasses. The obtained results illustrated that PbO and Bi_2O_3 oxides reduced the glass samples' mechanical properties. For instance, the bulks' model decreased between 68.15 and 44.10 GPa, the shear model also followed the same trend and decreased from 31.95 to 23.33 GPa, reducing the PbO and Bi_2O_3 ratios in the studied glass samples. Monte Carlo N-Particle Transport Code (MCNP-5) was utilized to evaluate the investigated glasses' shielding capacity. The obtained results depict that the highest linear attenuation coefficient (LAC) occurred at 0.356 MeV; it takes values 0.618, 1.024, 1.161, 1.271, 1.963, and 2.071 cm^{-1} for G1, G2, G3, G4, G5, and G6. Based on the simulated values of LAC, other shielding properties such as transmission rate (TR), radiation protection efficiency (RPE), half-value layer (HVL) were evaluated. The calculated results illustrated that the shielding properties enhanced with Bi_2O_3 and PbO insertion ratios.

* *Corresponding author.*
E-mail address: mhmzaid@upm.edu.my (M.H.M. Zaid).
https://doi.org/10.1016/j.jmrt.2021.01.117

1. Introduction

Radiation shielding technology has significantly improved over the last few decades due to an increased interest in this field. There are currently thousands of applications for radiation, varying from energy production to medicine [1]. Due to the more prominent use of radiation, workers are exposed to the effects of harmful ionization radiation more than ever. Contact with high-energy photons can be extremely dangerous, as it can lead to cell mutations, cancer, and even death [2]. Standard safety procedures are implemented to protect people commonly exposed to radiation, such as nuclear power plant workers or medical doctors and patients. The radiation exposure is minimized through three principles. By reducing the time under contract with the high-energy photons and maintaining a safe distance from the source, workers are already safer from the potentially harmful effects [3]. However, these first two guidelines cannot always be wholly followed, as workers and patients must come close to the source of radiation at times to complete a certain treatment, such as in X-ray rooms. In such cases, protective materials are used to absorb incoming radiation and reduce exposure [4]. Radiation shields vary depending on the source and use of the radiation; however, there are a few categories of commonly utilized materials. One of these is concrete. Concrete is commonly used to safely line the walls of nuclear reactors and store and contain nuclear waste. This material has a multitude of characteristics that are desirable for radiation shields, including a low cost of manufacture, varying structure, and structurally strong [5–7]. Concrete contains a mixture of light hydrogen nuclei and heavy nuclei (doping or aggregate). Thus, concrete samples can absorb or attenuate neutrons and gamma-rays effectively [8]. However, concretes also have some downsides, such as being prone to cracking and tend to lose water after prolonged exposure to radiation. Other categories of materials include alloys, composites, and glasses [9]. Each type of material has its pros and cons, but glasses have recently gained more attention due to their advantageous properties.

Glasses are commonly utilized as optical devices in electrical technologies, as transparent windows in x-ray rooms, for security applications, as well as others. They offer various desirable qualities, such as range of composition, low cost of manufacture, and transparency [10–13]. Impurities were introduced in the form of metals to turn common glass into a radiation shield glass. This doping, especially with heavy metal oxides, improves the glass's attenuation properties to be used as a shielding material. Glass formers are oxides that act as the backbone for the glass structure and are essential to the glass network. The six glasses investigated in this study are either silica or borate glasses, which are the two most common formers. One of the glasses is composed of cadmium oxide, a glass modifier that alters the glass network itself. Lead oxide, bismuth oxide, and aluminum oxide are added to the glasses in varying quantities to assess their glass network effects. These three oxides are glass intermediates that can function as either a network former or modifier, depending on the glasses' composition. They are added in order to improve the physical and radiation shielding properties of the samples.

Various parameters need to be calculated to determine the attenuating ability of the glasses. The most important parameter, mass attenuation coefficient (MAC), describes the amount of radiation absorbed by the sample and is utilized to calculate other parameters, such as half-value layer (HVL) and mean free path (MFP). Other parameters were calculated, such as linear attenuation coefficient (LAC), transmission rate, and radiation protection efficiency (RPE%). Waly et al. [10] used MicroShield code and reported the radiation attenuation features for different oxide glasses between 0.015 and 15 MeV. They found that these glasses have very interesting shielding properties due to the high density of the glasses. We aimed in this paper to extend this work for two reasons: (1) we selected some energies such as 0.356, 0.662, 1.173 and other energies which used in real applications, and (2) we reported the mechanical properties to determine the range of usefulness of these glasses in real shielding applications Makishima-Mackenzie elastic model was employed to calculate theoretical values for the elastic moduli of the current glass samples. Additionally, the MCNP code was used to report the mass attenuation coefficient for the tested glasses.

2. Material and methods

2.1. *Makishima-Mackenzie elastic modeling*

The Makishima-Mackenzie elastic model can be utilized to estimate theoretical values for the elastic properties of oxide glasses [14]. The elastic modulus (or plural moduli) is a measure that describes the stiffness of a material when a certain force is exerted upon it. This model can measure the elastic moduli of the various glass types in terms of their chemical composition. The calculation required information about the packing density and the dissociation energy (G_i) of the glass oxides. Generally, the packing density values can be discovered using the equations [15]:

$$V_t = \frac{\rho}{M}\sum_i x_i V_i \tag{1}$$

where V_i is given by

$$V_i = \frac{4\pi N_A}{3}\left(x r_M^3 + y r_O^3\right) \tag{2}$$

where:

N_A: Avogadro's number
r_M: cation ionic radii of the oxide M_xO_y
r_O: anion ionic radii of the oxide M_xO_y

The elastic moduli and the Poisson's ratio of the glasses can be measured using the following relation:

Table 1 – Compositions by weight% and density of the six investigated glasses.

Sample	Density (g/cm^3)	PbO	Al_2O_3	B_2O_3	SiO_2	CdO	Bi_2O_3
G1	4.377	0.25	0.1	0.65	–	–	–
G2	5.791	0.45	0.1	0.45	–	–	–
G3	6.220	0.5	0.1	–	0.4	–	–
G4	7.726	0.3	–	0.2	–	0.5	–
G5	7.801	0.3	–	0.2	–	–	0.5
G6	8.284	0.8	0.1	–	0.1	–	–

$$E_{MM} = 2V_t \sum_i G_i x_i \quad (3)$$

$$K_{MM} = 1.2\ V_t E_{MM} \quad (4)$$

$$G_{MM} = \frac{3E_{MM}K_{MM}}{9K_{MM}} - E_{MM} \quad (5)$$

$$\sigma_{MM} = \frac{E_{MM}}{2G_{MM}} - 1 \quad (6)$$

2.2. Monte Carlo simulation

The Monte Carlo N-Particle Transport code is a non-distractive tool (MCNP5) used to evaluate the studied G1-G6 glasses' shielding factors at six different gamma photon energies between 0.356 and 1.408 MeV. The composition and density of the studied G1-G6 glasses were introduced to the input file in the material and surface card section. The composition and density of the tested G1-G6 glasses are listed in Table 1. The input file also contains all the required information about the geometry (Cell and surface cards). The geometry used in the current simulation process is illustrated in a 3-D view in Fig. 1. In the 3D geometry presented in Fig. 1, the gamma source emits 10^6 photons/min along the +Z direction and is placed 100 mm away from the lead collimator. This collimator is 15 cm high and contains a cylindrical slit of 20 mm in diameter. The studied G1-G6 glasses were placed at a distance of 30 mm away from the lead collimator. Furthermore, the detector was placed 30 mm from the studied glasses and set up to be tally F4 to record the incoming photons' average track length inside the studied glasses. The simulation was carried out, and the achieved results have a relative error of less than 1%, as presented in the MCNP5 output sheets of MCNP5 code [16,17].

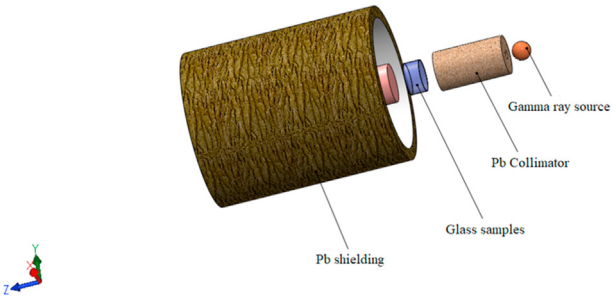

Fig. 1 – The geometry used in the simulation process.

2.3. Calculation of the radiation shielding capacity

The incoming gamma photon's average track length was simulated using a useful nondestructive Monte Carlo Simulation code (MCNP-5). Based on the simulated average track length, some important shielding factors were calculated as the following [18–20]:

$$LAC = \mu\ (cm^{-1}) = \frac{1}{t}\ln\left(\frac{I_o}{I}\right) \quad (7)$$

$$MAC = \mu_m (cm^2\ g^{-1}) = \frac{\mu\ (cm^{-1})}{\rho\ (g\ cm^{-3})} \quad (8)$$

$$Transmission\ rate = \frac{I}{I_o} = \exp(-\mu\ t) \quad (9)$$

$$MFP\ (cm) = \frac{1}{\mu\ (cm^{-1})} \quad (10)$$

$$HVL = \frac{\ln(2)}{\mu\ (cm^{-1})} \quad (11)$$

$$RPE(\%) = (1 - \exp(-\mu t))*100 \quad (12)$$

where:

I_o: the incoming photon intensity
I: the transmitted intensity
LAC or μ: linear attenuation coefficient
MAC or μ_m: mass attenuation coefficient
t: the thickness of the shielding material
ρ: density of the shielding material
HVL: the half-value layer
MFP: mean free path
RPE: the radiation protection efficiency

The dose rate received by a radioactive source placed at a distance d from exposure without a shielding material can be described by equation (6).

$$\text{Dose rate}\ \left(\frac{Sv}{h}\right) = \frac{\Gamma\ A}{d^2} \quad (13)$$

where Γ and A represent the specific gamma-ray constant and the radioactive source activity, if a material with thickness t and LAC μ shielded the radioactive source, the previous equation (7) could be modified and written as.

$$Dose\ rate = \frac{\Gamma\ A}{d^2}\ \exp(-\mu_{glass}\ t) \quad (14)$$

Table 2 – Variation of elastic moduli and Poisson's ratio calculated using Makishima-Mackenzie elastic model.

Sample	Density (g/cm^3)	K_{MM} (GPa)	G_{MM} (GPa)	L_{MM} (GPa)	E_{MM} (GPa)	σ_{MM}
G1	4.377	68.15	31.95	111.13	82.89	0.30
G2	5.791	57.51	27.29	95.32	71.50	0.29
G3	6.220	49.59	26.05	84.11	66.38	0.28
G4	7.726	46.12	25.04	79.67	63.89	0.27
G5	7.801	45.45	24.45	78.06	62.19	0.27
G6	8.284	44.10	23.33	74.90	59.50	0.27

3. Results and discussion

3.1. *Elastic properties*

The addition of PbO and heavy metal oxides such as CdO and Bi_2O_3 causes a drastic change in the glasses' structure. The addition of oxides, such as PbO, CdO, and even Bi_2O_3, with high atomic masses, leads to a sharp increase in the glass density, thus reducing the elastic moduli. The substitution of heavy metal oxides provides oxygen ions in the glass precursor that allow it to change. For G1 and G2, there are numerous trigonal bipyramid BO_4 through the changes of BO_{3+1} from trigonal pyramid BO_3. It seems that increasing the PbO concentration enhances the B–O connection, strengthening the glass structure networks while decreasing the hardness of the glass sample. The addition of PbO content to the glass system start to break a bond and increase the progress of non-bridging oxygens (NBO's). The borate network becomes even more homogenized due to the uniform Pb^{2+} ions distribution in the B–O chains of the glass matrix as some of the B_2O_3 ions still connect by sharing the same edge [19]. For glass samples, G3, G4, G5, and G6, the addition of heavy metal oxides such as CdO and Bi_2O_3 resulted in a more linear increase in density, which led to a significant decrease in the elastic moduli. These elastic moduli reductions were achieved by increasing the average cross-link density, associated with a reduction in the dissociation energy (G_i), as shown in Table 2 and Fig. 2. Fig. 2

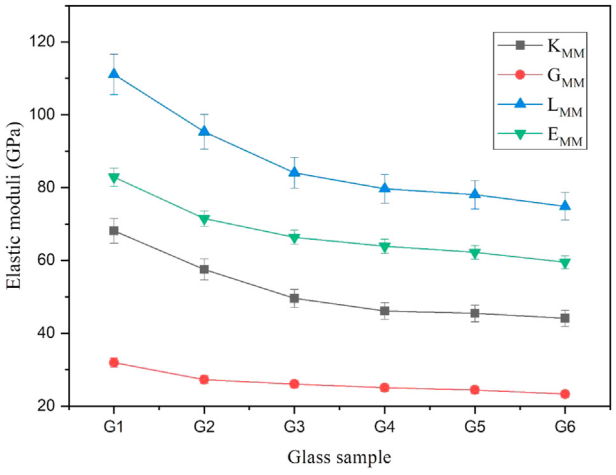

Fig. 2 – Variation of elastic moduli of glasses calculated using Makishima-Mackenzie elastic model.

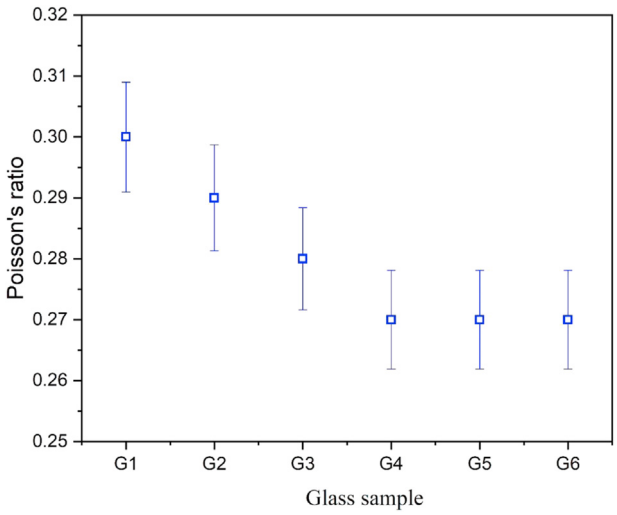

Fig. 3 – Poisson's ratio of glasses calculated using Makishima-Mackenzie elastic model.

shows that the K_{MM} decreases from 68.15 to 44.10 GPa as there is an increase in the PbO, CdO, and Bi_2O_3 concentration. Another elastic modulus that has the same trend, G_{MM}, decreases from 31.95 to 23.33 GPa, while L_{MM} decreases from 111.13 to 74.90 GPa. The mentioned reduction trend also occurred for the E_{MM} calculation, in which the calculated values decreased from 82.89 to 59.50 GPa. The Poisson (σ_{MM}) ratio is one of the most important data for measuring the materials' mechanical properties. Poisson ratio explains the longitudinal strain sections formed by the pressure-sensitive. In Fig. 3, the calculation σ_{MM} values are in the range between 0.30 and 0.27, as presented in Table 2. These values prove that the cross-link density is connected through the medium resistance with the direction of lateral expansions. The reduction trend in the σ_{MM} values occurs due to heavy metal oxide insertions into the glass matrix. This change is also associated with the rise in the actual cross-link density, which

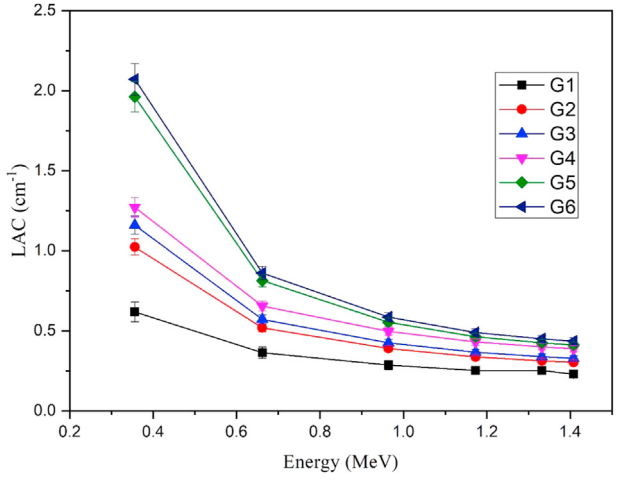

Fig. 4 – The variation of the linear attenuation coefficient (LAC) of the studied glasses versus the incident gamma photon energies.

Table 3 – The mass attenuation coefficient of the studied glasses.

Energy (MeV)	The mass attenuation coefficient ($cm^2 g^{-1}$)															
	G1			G2			G3			G4			G5			G6		
	MCNP	XCOM	Diff (%)	MCNP	XCOM	Diff (%)	MCNP	XCOM	Diff (%)	MCNP	XCOM	Diff (%)	MCNP	XCOM	Diff (%)	MCNP	XCOM	Diff (%)
0.356	0.141	0.142	0.339	0.177	0.177	0.087	0.187	0.187	0.144	0.165	0.164	0.490	0.252	0.240	4.757	0.250	0.239	4.445
0.662	0.083	0.084	0.319	0.090	0.090	0.437	0.092	0.092	0.467	0.085	0.085	0.436	0.104	0.102	2.399	0.104	0.102	2.276
0.964	0.066	0.066	0.260	0.067	0.068	0.347	0.068	0.069	0.369	0.064	0.065	0.336	0.071	0.071	0.498	0.071	0.071	0.474
1.173	0.058	0.059	1.141	0.058	0.059	1.809	0.059	0.060	1.999	0.056	0.057	2.002	0.059	0.061	2.906	0.059	0.061	2.966
1.332	0.058	0.054	5.927	0.054	0.055	1.526	0.055	0.056	1.689	0.052	0.053	1.685	0.055	0.056	2.468	0.054	0.056	2.517
1.408	0.052	0.053	0.912	0.052	0.053	1.453	0.053	0.054	1.591	0.050	0.051	1.602	0.053	0.054	2.337	0.053	0.054	2.379

contributed to the intensification of NBO's in the glass structure, weakening the glass network.

3.2. *Radiation shielding capacity*

The gamma photons' average track length was used to calculate the linear attenuation coefficient (LAC) for the investigated glasses. The LAC was simulated for at selected energies: 0.356, 0.662, 0.964, 1.173, 1.332 and 1.408 MeV. The simulated LAC was plotted versus the gamma photon energy, as shown in Fig. 4. Generally, the LAC values for the studied glasses agree with the Lambert–Beer law. Thus, the calculated values of LAC decrease exponentially with photon energy. Among the selected energy range, the highest LAC obtained for all studied glasses was at 0.356 MeV and varied between 0.618 and 2.072 cm^{-1}, respectively. In contrast, the lowest LAC values were achieved around the gamma energy of 1.408 MeV. It is varied between 0.228 and 0.436 cm^{-1} for glasses G1 and G6. After that, the LAC's simulated values were observed to decrease gently with gamma photon energies. The slow reduction in the LAC values is due to the Compton scattering phenomena in the intermediate energy zone [20,21]. It is clear that the LAC reduction for glasses G1, G2, and G3 are higher than the reduction observed for glasses G6 and G5. This trend can be related to the high contents of PbO and Bi_2O_3, which represent around 80 wt% of the G6 and G5 contents. Glasses G5 and G6 possess the highest shielding capacity among the studied glasses. These good shielding capacities are due to their high densities, where the density of the G5 glass is around 7.801 g cm^{-3} and the density of glass G6 around 8.284 g cm^{-3}. On the other hand, the lowest shielding capacity among the selected glasses can be attributed to G1, which has a density of around 4.376 g cm^{-3}.

The average track length of the gamma rays in the studied glasses was used to calculate the MAC for gamma photons with energies in the range between 0.356 and 1.498 MeV. Values of the MAC were calculated based on the simulated results and were compared to the data calculated using the XCOM database [22,23], as illustrated in Table 3. It is observed that the simulated MAC values are close to the results calculated using the XCOM database. For instance, the MCNP and XCOM values of MAC for G1 at 0.356 MeV are 0.141 and 0.142 cm^2/g respectively, while those values at 0.662 MeV for the same glass are 0.083 and 0.84 cm^2/g. Also, for G4 (as aan example), the simulated and XCOM values are 0.056 and 0.057 cm^2/g (this is at 0.662 MeV), while at 1.408 MeV they are 0.050 and 0.051 cm^2/g. The difference (%) between the simulated and calculated MAC was calculated according to equation (15).

$$Diff(\%) = \frac{[(MAC)_{MCNP} - (MAC)_{XCOM}]*100}{(MAC)_{MCNP}} \quad (15)$$

The difference (%) in MAC values between the MCNP and XCOM data varied between 0.08 and 4.45%. Table 3 depicts that the highest MAC was obtained for glass with 80 wt % of PbO content (G6). It is increased between 0.053 and 0.250 $cm^2\ g^{-1}$. On the other hand, the lowest MAC was obtained for glass with 25 wt% of PbO (G1). It is varied from 0.052 to 0.141 $cm^2\ g^{-1}$ with increasing the gamma-photon energy

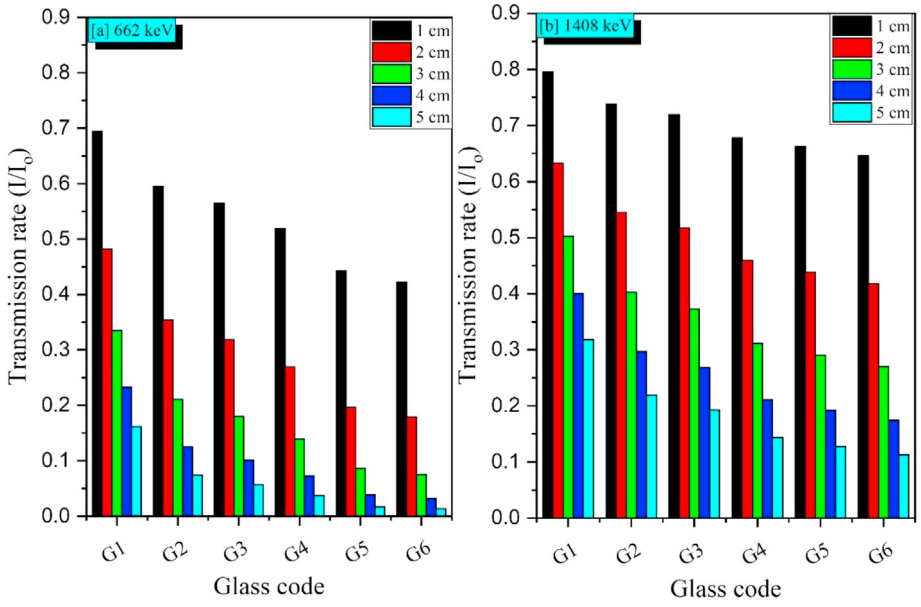

Fig. 5 – The gamma photons transmission rate at 0.662 and 1.408 MeV for the studied glasses.

between 0.356 and 1.408 MeV [17]. It can be observed that the G5 glasses with 30 wt% PbO and 50wt % Bi_2O_3 content have MAC values equal to the MAC of the G6 glasses, which possess 80 wt % PbO contents.

The transmission factor of the studied G1-G6 glasses was computed at various thicknesses for the materials, in the range of 1–5 cm. Fig. 5 depicts the variation of the transmission factor versus the glasses thickness for some fixed gamma photon energies (for 0.662 and 1.408 MeV). Two interesting points were observed in Fig. 5. The first point is that the number of incoming photons that penetrate the studied G1-G6 glasses increases with increasing photon energy. Thus, the studied G1-G6 glasses' transmission factor increases with the increase in the incoming photon energy. For example, the transmission factor for glasses G1 with thickness 1 cm is 0.694 at 0.662 MeV, while it is 0.795 at 1.408 MeV. This means that for G1 glass with a thickness of 1 cm, about 69% of the incoming photons with energy of 0.662 MeV can penetrate this glass, wile for the same glass, about 80% of the photons with energy of 1.408 MeV (most of the photons) can penetrate this glas. On other words, we can say that the glass is a good shield when exposed to a photons with relatively low energy. The second point is that the transmission factor decreases systematically with increasing the glass thickness. For example, the transmission rate of gamma photons with energies of 0.662 MeV through a thickness of 1 cm is equal to 0.422, while the transmission rate for the same photon energy through 5 cm is equal to 0.013 for glass G6. In this regard, it can be concluded that the highest transmission rates are obtained at smaller thicknesses. The

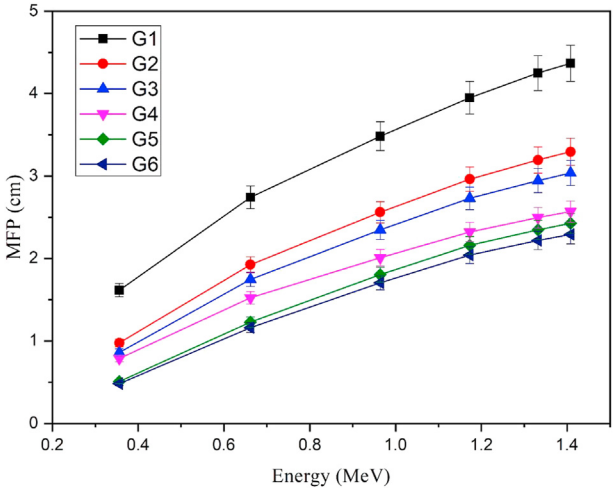

Fig. 6 – The variation of the MFP of the studied glasses versus the incident gamma photon energy.

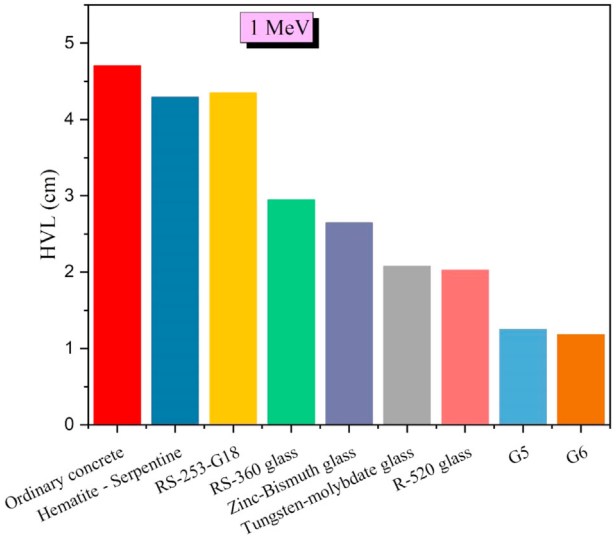

Fig. 7 – Comparison between the HVL of the studied glasses (G5 and G6) and other shielding materials such as concretes and commercial glasses.

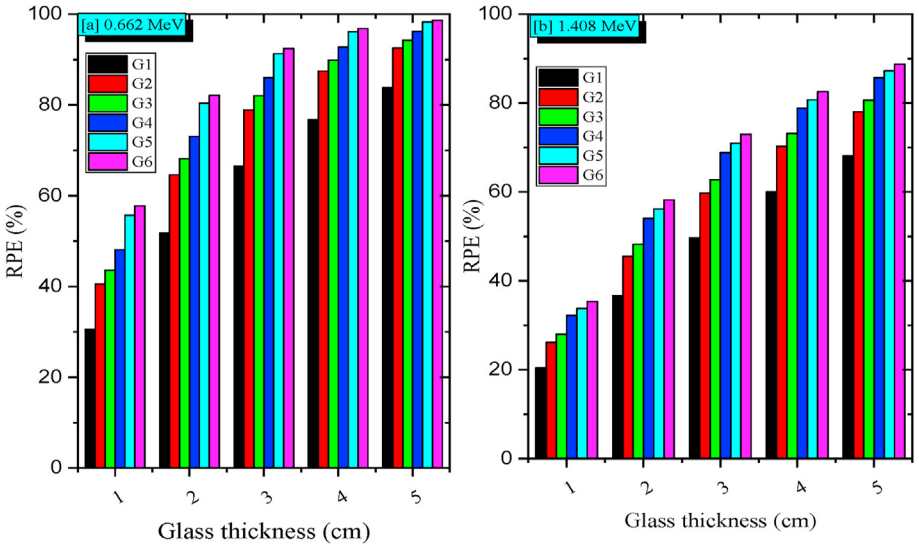

Fig. 8 – The variation of the radiation protection efficiency of the studied glasses as a function of the glass thickness.

small thickness is not enough for more interactions between the glass atoms and the incoming gamma photons. A small part of the incoming photon energy is lost during the interaction. Thus, the incoming photons still have high penetration power and easily penetrate through the small thicknesses. The lowest transmission rate was achieved at a thicker glass thickness (x = 5 cm). For large thicknesses, the incoming gamma photons have many interactions with the atoms of the material, and in each interaction, the photons lose a part of their energies. Thus, the large thicknesses' penetration is quite difficult, and the incoming photons lose a large part of their energies.

The mean free path (MFP) is the parameter used to predict the distance in which the incoming gamma photon travels inside the glasses between the two following interactions. Fig. 6 illustrates the variation of the MFP of the studied G1-G6 glasses versus the gamma photon energy. The lowest values of the MFP were obtained at a gamma photon energy of 0.356 MeV and varied in the range between 0.482 cm for glasses G6 and 1.615 cm for glasses G1. After that, the predicted values of the MFP of the studied G1-G6 glasses progressively increased with the increase in the incoming gamma photon energy. This increase is due to Compton scattering, which is the main interaction in the selected energy range of 0.356–1.408 MeV [24]. Values of the MFP were observed to increase rapidly with an increase in the incoming energy for glasses with low PbO contents (for G1, G2, and G3 glass samples), while the predicted values of the MFP increase slowly with an increase in the incoming energy for glasses with high contents of PbO and Bi_2O_3 (for G5 and G6 glasses). Fig. 6 shows that the insertion of PbO and Bi_2O_3 has a considerable improvement in the MFP of the studied G1-G6 glasses. The predicted MFP's highest values were achieved for gamma photons with an energy of 1.408 MeV and varied in the range between 2.291 cm for G6 glasses and 4.367 cm for G1 glasses.

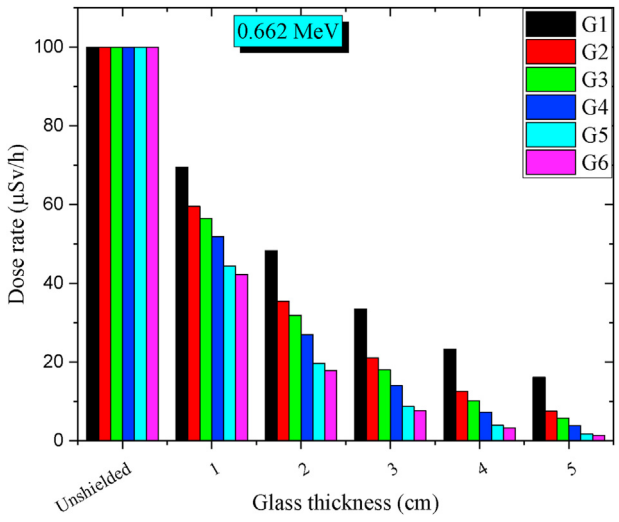

Fig. 9 – Variation of the dose rate of ^{137}Cs source as a function of the shielding thickness.

The half-value layer of the studied G1-G6 glasses was calculated at gamma photon energies in the range of 0.536–1.408 MeV. The thicker HVL was observed for the G1 glasses with a content of 25 wt% of PbO and varied between 1.119 and 3.026 cm, while the thinner HVL is obtained for G6 glasses with a content of 80 wt% PbO and G5 glasses with contents 30 wt% PbO in addition to 50 wt% Bi_2O_3. The HVL of the studied glasses (for example, G5 and G6 samples) was compared to the HVL of some commercial shielding materials such as ordinary concretes [25], concretes with hematite-serpentine minerals [26], tungsten molybdenum tellurite glass [27], zinc bismuth borate glass [28] and SCHOTT radiation shielding glasses (RS-253-G18, RS-360, and RS-520) [29] as illustrated in Fig. 7. The HVL of ordinary concrete was considered the highest, where a thickness of 4.702 cm is required to absorb half of the incoming photons with an energy of 1 MeV. The HVL of the concretes with hematite-serpentine minerals are equal to 4.291 cm and is similar to

the HVL of the SCHOTT glasses RS-253-G18. The lowest thickness required to absorb the incoming gamma photons with an energy of 1 MeV is 1.250 cm for G5 and 1.181 cm for G6 glasses.

The radiation protection efficiency (RPE) for the G1-G6 glasses was calculated at two gamma-ray energies, 0.662 and 1.408 MeV (for examples). The calculated results were plotted in Fig. 8. Three important points can be observed through this figure. The first deals with the increase of the RPE with the increase of the glass thicknesses. For glasses G1 (for example) at the gamma photon energy 0.662 MeV, the RPC for a 1 cm thickness is equal to 30.56%, while for thickness 5 cm, the RPE is 83.85%. In the thinner thicknesses of the studied G1-G6 glasses, the incoming photons could not make enough interactions with the glass atoms, so only a small part of the gamma-ray energy was absorbed. Thus, the RPE possesses lower values at thinner thicknesses. With thicker thicknesses, however, the incoming photons have many interactions with the glass atoms. A large part of the incoming photon energy is absorbed inside the studied glasses, so a small number of photons can penetrate through the glass. Thus, the RPE increased for the thicker glasses. The second point deals with the incoming photon energy, where the RPE was observed to increase with the increase of the incoming photon's energy. An increase in photon energy leads to an increase in the photons' penetration power, so it is easier for the incoming photons to penetrate through the material. The third point deals with the glass structure where the RPE was observed to increase with the increase of heavy metal contents in the glass. Thus, the RPE for glasses G6 with PbO contents 80 wt % is higher than the RPE of the glasses G1 with PbO contents 25 wt%. An increase of the glass's heavy metals leads to an increase in the effective atomic number of the studied glass, which increases the probability and cross-section of gamma photon interactions.

The dose rate received from the unshielded gamma-ray source ^{137}Cs is 100 μSv/h. The selected gamma-ray source is placed at a distance of 100 cm from the exposed materials. The variation of the dose rate versus the glass thickness was calculated and illustrated in Fig. 9. The dose rate was observed to decrease with an increase in the glass thickness, where the dose rate for glasses G6 (for example) was 42.263, 17.861, 7.548, 3.190, and 1.348 μSv/h for thicknesses of 1, 2, 3, 4, 5 cm. In terms of the chemical composition, the dose rate was observed to decrease with the increase of heavy metal contents in the studied G1-G6 glasses. The highest dose rate received was recorded for the G1 glasses and varied between 16.145 μSv/h for a thickness of 5 cm and 69.439 μSv/h for a thickness of 1 cm. On the other hand, the lowest dose rate received by exposures was recorded for the G6 glasses and varied between 1.348 μSv/h for the glass thickness of 5 cm and 42.263 μSv/h for the glass thickness of 1 cm.

4. Conclusion

The results demonstrate that the addition of heavy metal oxides such as PbO increases the mechanical properties and radiation shielding abilities of the investigated glasses. Makishima-Mackenzie's model revealed that as the density of the glasses increased, their elastic moduli decreased with it. When considering K_{MM}, G_{MM}, L_{MM}, and E_{MM}, G6 was observed to have the least elastic values out of the other investigated glasses. Various radiation shielding parameters were calculated, including LAC, MAC, MFP, HVL, TF, RPE, and dose rate. G1 indicated the worst attenuation characteristics when considering these parameters, increasing as the glasses increase from G1-G6. Overall, the G6 glass was proven to be the most effective radiation shielding glass out of the investigated samples and has the most potential to be utilized for shielding applications.

CRediT authorship contribution statement

M.H.M. Zaid: Writing - original draft, Funding acquisition, Supervision. **H.A.A. Sidek:** Conceptualization, Funding acquisition. **K.A. Matori:** Conceptualization, Writing - original draft. **A. Abdu:** Conceptualization. **K.A. Mahmoud:** Conceptualization, Methodology, Investigation, Writing - original draft. **Maha M. Al-Shammari:** Investigation. **E. Lacomme:** Conceptualization, Methodology. **Mohammad A. Imheidat:** Conceptualization, Methodology. **M.I. Sayyed:** Conceptualization, Methodology, Writing - original draft.

Declaration of Competing Interest

There are no conflicts of interest to declare.

Acknowledgment

The authors express their gratitude to the Universiti Putra Malaysia for support in the present investigation.

REFERENCES

[1] Pillai M, Adapa K, Das SK, Mazur L, Dooley J, Marks LB, et al. Using artificial intelligence to improve the quality and safety of radiation therapy. J Am Coll Radiol 2019;16:1267–72.
[2] Al-Hadeethi Y, Sayyed MI, Rammah YS. Fabrication, optical, structural and gamma radiation shielding characterizations of GeO_2-PbO-Al_2O_3–CaO glasses. Ceram Int 2020;46:2055–62.
[3] Jemes EM. Principles of radiological health and safety. 1st ed. New Jersey: John Wiley Sons, INC Hoboken; 2003.
[4] Reiss J, O'Connell H, Getman MK. Achieving contrast-free ultra-low radiation exposure without compromising safety and acute efficacy through evolving AF cryoballoon ablation procedure techniques. Int J Cardiol 2020;299:153–9.
[5] Zayed AM, Masoud MA, Rashad AM, El-Khayatt AM, Sakr K, Kansouh WA, et al. Influence of heavyweight aggregates on the physico-mechanical and radiation attenuation properties of serpentine-based concrete. Construct Build Mater 2020;260:120473.
[6] Waly ESA, Mohamed AB. Comparative study of different concrete composition as gamma-ray shielding materials. Ann Nucl Energy 2015;85:306–10.

[7] Masoud MA, Kansouh WA, Shahien MG, Sakr K, Rashadd AM, Zayed AM. An experimental investigation on the effects of barite/hematite on the radiation shielding properties of serpentine concretes. Prog Nucl Energy 2020;120:103220.
[8] Gencel O, Bozkurt A, Kam E, Korkut T. Determination and calculation of gamma and neutron shielding characteristics of concretes containing different hematite proportions. Ann Nucl Energy 2011;38:2719–23.
[9] Al-Hadeethi Y, Sayyed MI, Mohammed Hiba, Rimondin Lia. X-ray photons attenuation characteristics for two tellurite based glass systems at dental diagnostic energies. Ceram Int 2020;46:251–7.
[10] Waly El-Sayed A, Fusco Michael A, Bourham Mohamed A. Gamma-ray mass attenuation coefficient and half value layer factor of some oxide glass shielding materials. Ann Nucl Energy 2016;96:26–30.
[11] Halimah MK, Azuraida A, Ishak M, Hasnimulyati L. Influence of bismuth oxide on gamma radiation shielding properties of boro-tellurite glass. J Non-Cryst Solids 2019;512:140–7.
[12] Rashad AM. Recycled cathode ray tube and liquid crystal display glass as fine aggregate replacement in cementitious materials. Construct Build Mater 2015;93:1236–48.
[13] Al-Hadeethi Y, Sayyed MI. $BaO–Li_2O–B_2O_3$ glass systems: Potential utilization in gamma radiation protection. Prog Nucl Energy 2020;129:103511.
[14] Makishima A, Mackenzie JD. Calculation of bulk modulus, shear modulus and Poisson's ratio of glass. J Non-Cryst Solids 1975;17:147–57.
[15] Saddeek YB, Bashier A, Bakr SA. Theoretical analysis of constants of elasticity of lead calcium alumino borosilicate glass system. Glass Phys Chem 2012;38:437–43.
[16] Sayyed MI, Mohammed Faras Q, Mahmoud KA, Lacomme Eloic, Kaky Kawa, Khandaker Mayeen, et al. Evaluation of radiation shielding features of Co and Ni-based superalloys using MCNP-5 code: potential use in nuclear safety. Appl Sci 2020;10:7680.
[17] Divina R, Marimuthu K, Mahmoud KA, Sayyed MI. Physical and structural effect of modifiers on dysprosium ions incorporated boro-tellurite glasses for radiation shielding purposes. Ceram Int 2020;46:17929–37.
[18] Dong MG, Sayyed MI, Lakshminarayana G, Ersundu MÇ, Ersundu AE, Nayar P, et al. Investigation of gamma radiation shielding properties of lithium zinc bismuth borate glasses using XCOM program and MCNP5 code. J Non-Cryst Solids 2017;468:12–6.
[19] Effendy N, Sidek HAA, Kamari HM, Zaid MHM, Wahab SAA. Ultrasonic and artificial intelligence approach: elastic behavior on the influences of ZnO in tellurite glass systems. J Alloys Compd 2020;835:155350.
[20] Elbashir BO, Dong MG, Sayyed MI, Issa SA, Matori KA, Zaid MHM. Comparison of Monte Carlo simulation of gamma ray attenuation coefficients of amino acids with XCOM program and experimental data. Results Phys 2018;9:6–11.
[21] Abouhaswa AS, Sayyed MI, Mahmoud KA, Al-Hadeethi Y. Direct influence of mercury oxide on structural, optical and shielding properties of a new borate glass system. Ceram Int 2020;46:17978–86.
[22] Seltzer SM. Calculation of photon mass energy-transfer and mass energy-absorption coefficients. Radiat Res 1993;136:147.
[23] Berger MJ, Hubbel H, Seltzer SM, Chang J, Coursey JS, Sukumar R, et al. XCOM: photon cross sections database. 2010.
[24] Abouhaswa AS, Sayyed MI, Al-Hadeethi Y, Altowyan AS, Mahmoud KA. Evaluation of optical and gamma ray shielding features for tungsten-based bismuth borate glasses. Opt Mater 2020;106:109981.
[25] Bashter II. Calculation of radiation attenuation coefficients for shielding concretes. Ann Nucl Energy 1997;24:1389–401.
[26] Bashter II, Makarious AS, Abdo ES. Investigation of hematite-serpentine and ilmenite-limonite concretes for reactor radiation shielding. Ann Nucl Energy 1996;23:65–71.
[27] Ersundu AE, Büyükyıldız M, Çelikbilek Ersundu M, Şakar E, Kurudirek M. The heavy metal oxide glasses within the WO_3-MoO_3-TeO_2 system to investigate the shielding properties of radiation applications. Prog Nucl Energy 2018;104:280–7.
[28] Yasaka P, Pattanaboonmee N, Kim HJ, Limkitjaroenporn P, Kaewkhao J. Gamma radiation shielding and optical properties measurements of zinc bismuth borate glasses. Ann Nucl Energy 2014;68:4–9.
[29] El-Mallawany R, Sayyed MI, Dong MG, Rammah YS. Simulation of radiation shielding properties of glasses contain PbO. Radiat Phys Chem 2018;151:239–52.